# Characterization of critical residues in the extracellular and transmembrane domains of the endothelin type-B receptor for propagation of the endothelin-1 signal

*Tomoko Doi,[1*] Kohei Kikuta,[1†] and Kazutoshi Tani[2]*

[1] Department of Biophysics, Graduate School of Science, Kyoto University, Kyoto 606-8502, Japan.

[2] Graduate School of Medicine, Mie Un iversity, 2-174 Edobashi, Tsu, Mie 514-8507, Japan.

**ABSTRACT**

We previously reported the crystal structures of endothelin-1 (ET-1)-bound, ligand-free, and antagonist bosentan-bound forms of the thermostabilized ET type-B receptor ($ET_B$). Although other agonist-bound structures of $ET_B$ have been determined, the interactions for high-affinity binding and $ET_B$ receptor activation, as well as the roles of rearrangement of the hydrogen-bond network surrounding the ligand in G protein activation, remain elusive. ET-1, a 21 amino acid residue-long peptide, plays fundamental roles in basal vascular tone, sodium balance, cell proliferation, and stress-responsive regulation. We studied the interactions between the ET-1(8-21) peptide and $ET_B$ in the ligand binding and activation of $ET_B$ using a series of Ala-substituted ET-1(8-21) and the mutated $ET_B$. We found that while D8, L17, D18, I20, and W21 were responsible for high-affinity binding and potent G protein activation, Y13 and F14 in the helical region of ET-1 are prerequisites for the full activation of $ET_B$ via interactions near the extracellular side. Furthermore, we introduced the mutation into the residues around the ET-1 binding pocket of $ET_B$. The results showed that while $S184^{3.35}$, $W336^{6.48}$, $N378^{7.45}$, and $S379^{7.46}$ in a conserved polar network are required for full activation, $N119^{1.50}$, $D147^{2.50}$, and $N382^{7.49}$ are essential for G protein activation via direct interactions after rearrangement upon ET-1 binding. These results demonstrate that both interactions near the extracellular side and within the transmembrane helices with ET-1 play crucial roles in the full activation of the $ET_B$ receptor.

## INTRODUCTION

Endothelins (ETs), composed of three isopeptides, ET-1, -2, and -3, are ubiquitously expressed peptide hormones with unique cyclic structures via two intramolecular disulfide bonds[1]. They exert a number of physiological functions, including the regulation of vascular tone and cell proliferation, as well as the development of pathophysiological conditions, such as cardiovascular disease, heart failure, and cancer[2]. They act through ET receptors, subtypes $ET_A$ and $ET_B$, which are β-subfamily, class-A G protein-coupled receptors (GPCRs).

GPCRs mediate cellular responses to a diverse array of molecules outside the cell, including lipids, nucleosides, neurotransmitter, hormones, and proteins. Ligand binding triggers structural changes of GPCRs and initiates signal transmission. The molecular basis of peptide agonist-mediated GPCR activation is of great interest for the understanding of how the binding of a peptide agonist causes intracellular helical rearrangements, compared to those of relatively small rigid ligands, such as adrenalin and adenosine[3,4]. There are more than 100 peptide-binding GPCRs in classes A and B, which bind various sizes of peptide ligands, ranging from pentapeptides to proteins of more than 100 amino acid residues[3]. Among these, structures of chemokine, neurotensin, endothelin, apelin, μ-opioid, and angiotensin receptors bound to endogenous peptide agonists or their derivatives have been determined by X-ray or cryo-EM in class A GPCRs, which provides new insight into peptide ligand binding and the activation of GPCRs[3,5-8]. However, how peptide ligands interacting with various portions of GPCRs proceed conformational changes remains elusive.

We previously determined the crystal structures of ET-1-bound, ligand-free, and antagonist bosentan-bound forms of the thermostabilized $ET_B$ receptor[9,10]. In the ET-1-bound structure, multiple well-arranged interactions mediate ET-1-$ET_B$ binding over a wide surface area of $ET_B$, in

which the central region (8-17) of ET-1 forming a helical structure interacts with the N-terminal tail, extracellular loops (ECLs), and transmembrane helices of $ET_B$, and the C-terminal region (18-21) in an extended conformation that penetrates the transmembrane region of the receptor with the C-terminal tryptophan located most deeply, while the N-terminal region (1-7) is anchored to the helical region by two disulfide bonds.

Single mutations of $ET_B$ involved in these interactions with ET-1 decrease affinities, but the reduction in affinities is within less than one-tenth of the wild-type[9]. Therefore, interactions in which high-affinity binding and receptor activation are ascribed are not clear. To investigate the roles of ET-1-$ET_B$ interactions, we utilized a series of alanine-substituted ET-1(8-21) analogs and examined their binding affinities for $ET_B$ and $G_i$ activation efficiencies via $ET_B$. Furthermore, to confirm their interactions between $ET_B$ and ET-1 that are responsible for full activation, the $G_i$ activation of mutant receptors was examined using mammalian cell membranes co-expressing mutant receptors and the $\alpha_i$ subunit of G protein[11]. The results reveal previously unappreciated interactions between Y13 and F14 in the α-helical region of ET-1, and $P93^{N\text{-term}}$ and $I94^{N\text{-term}}$ in the N-terminal tail and $L361^{7.28}$ and $L364^{7.31}$ [superscripts indicate Ballesteros-Weinstein numbers[12]] in the TM7 of $ET_B$, respectively, which are important for full activation. These interactions induce inward movements of the N-terminal tail and the extracellular side of TM7, propagating the transmembrane helices.

In addition, a comparison of the ET-1-bound $ET_B$ structure with ligand-free and antagonist-bound structures suggests the helical movements of the transmembrane 1 (TM1) outward, and TM2, TM6, and TM7 inward on the extracellular side of the receptor upon binding of ET-1 (Figure S1B). Coupled with these movements, rearrangements of the conserved water-mediated hydrogen-bond network were observed around the ligand-binding pocket in various GPCR crystal

structures[13,14]. Furthermore, we studied how the conserved residues forming a polar network around the transmembrane ET-1 binding pocket contributed to $ET_B$ activation by the $G_i$ coupling of mutant receptors. The results suggest that the formation of the conserved polar network is important for the full activation of $ET_B$ and, in particular, the direct interactions between $N119^{1.50}$ and $D147^{2.50}$ and between $D147^{2.50}$ and $N382^{7.49}$ after the exclusion of a water molecule are crucial for G protein activation.

Here, we report the identification of residues Y13 and F14 of ET-1, responsible for the inward movement of the N-terminal tail and the extracellular side of TM7, which could provide insights into the requirements for agonists of the $ET_B$ receptor and shed light on the mechanism of activation. In particular, the C-terminal region of ET-1 is responsible for high affinity binding and introduces compact helical interactions in the $ET_B$ via rearrangement of the hydrogen-bond network. However, the binding of residues Y13 and F14 in the helical region of ET-1 is a prerequisite for its full activation. Both interactions collaborate to reorganize the polar network and shift the structural equilibrium to active conformation of the $ET_B$ receptor.

## EXPERIMENTAL PROCEDURES

**Materials ET-1** ($NH_2$-CSCSSLMDKECVYFCHLDIIW-COOH with two disulfide bonds between C1-C15 and C3-C11) was purchased from the Peptide Institute (Osaka). Peptide analogs were purchased from Eurofins. N-acetyl-[$Ala^{11,15}$]-ET-1(8-21), in which the sequence corresponds to the 8-21 of ET-1 and the disulfide-forming cysteines at positions 11 and 15 are substituted to alanine, was used as a template wild-type ET-1(8-21). The mutated peptide residues at positions 8, 9, 10, 12, 13, 14, 16, 17, 18, 19, 20, and 21 of ET-1 were replaced with alanine individually (Table S1). Peptides were dissolved in 0.1% acetic acid with sonication and mixing and quantitated with the molar absorption coefficient at 280 nm of 5,500 for Y13A, 1,400 for W21A, and 6,900 for others and ET-1[15].

**Reconstitution of F6hNET$_B$R into HDL (high-density lipoprotein) particles** Wild-type F6hNET$_B$R and mutant constructs containing an amino-terminal Flag-epitope tag followed by a hexa-histidine tag, were expressed in Sf9 insect cells using the Bac-to-Bac baculovirus system (Thermo Fisher Scientific) in 300~700 ml medium, as described[9]. Cells were solubilized in 1% digitonin and flag-ET$_B$Rs were purified using Flag-M2 resin (Sigma-Aldrich) and subsequent TALON Metal affinity resin (Takara Bio) in 0.1% digitonin, 20 mM Tris-HCl (pH 7.5), 0.3 M NaCl, and 100 mM imidazole. Recombinant apolipoprotein A-I (apoA-I), named membrane scaffold protein1 (MSP1) using the MSP1E3D1 construct (Addgene) was expressed in *Escherichia coli* and purified with Ni-NTA affinity resin (Quiagen)[16]. Flag-ET$_B$Rs were reconstituted into HDL particles according to the published methods[17,18], in which monomeric GPCRs were incorporated per reconstituted HDL particle, surrounded by a dimer of apoA-I. In brief, flag-ET$_B$Rs containing 50-100 pmol ligand binding activity in 200 μl volumes were incubated with 60-78 μM MSP1 and 7.5 mM POPC:POPG (3:2 molar ratio) for 1 h at 4°C. Detergent was removed via BioBeads

(BioRad) overnight at 4°C, and receptor-containing HDL particles were further isolated using Flag-resin (Figure S3).

**Radioligand binding assay** Peptide competition binding was initiated by the addition of HEK293 cell membranes containing the wild-type (6hNET$_B$) receptor (~1.2 fmol) to the assay mixture composed of 0.1% bovine serum albumin (BSA), 0.04-0.05 nM [$^{125}$I]ET-1 (2,200 Ci mmol$^{-1}$, PerkinElmer Life Sciences), and eight concentrations of unlabeled peptides (ranging from 10 pM to 30 μM) in 50 mM HEPES-NaOH, pH 7.5, 10 mM $MgCl_2$ (Mg-HEPES). Binding reactions of 50 μl were incubated at 37°C for 1 h and were terminated by dilution with cold Mg-HEPES, then were filtered onto glass fiber filters in 96-well plates (multiscreen HTS FB, Merck Millipore) to separate the unbound [$^{125}$I]ET-1. After three washes with cold Mg-HEPES, the radioactivity captured by the filters was counted using a γ-counter. Filters were pretreated with 0.1% BSA in Mg-HEPES. The results were analyzed by non-linear regression, using GraphPad Prism 6 software.

In the saturation binding assays, membranes or reconstituted HDL particles (rHDLs) containing ET$_B$ receptors were incubated with eight different concentrations of [$^{125}$I]ET-1 ranging from 2.0 to 200 pM in 50 μl of Mg-HEPES buffer containing 0.1% BSA at 37°C for 2 h. The receptors were isolated from the unbound [$^{125}$I]ET-1 and washed, and the amount of receptor-bound [$^{125}$I]ET-1 was measured as described above. The non-specific binding of [$^{125}$I]ET-1 in each reaction was assessed by including 100 nM ET-1 in the same reaction. The results were analyzed by fitting to a one-site binding equation, total and non-specific using the GraphPad Prism 6 software. Each experiment was performed two to four times. The $B_{max}$ values obtained were used as the concentration of ET$_B$ receptors.

**GTPγS binding assay** Wild-type and mutant $ET_B$ receptors in the rHDLs at 0.5~0.7 nM were preincubated with ~200 nM $G\alpha_{i1}$ (purified from *E. coli*) and ~140 nM $G\beta_1\gamma_2$ subunits (purified from Sf9 cells) at 4°C for 1 h in 20 mM HEPES-NaOH, pH 8.0, 1 mM EDTA, 100 mM NaCl, 10 mM $MgCl_2$ 1 mM dithiothreitol, and 1 μM GDP, as described previously[9]. Under these conditions, the receptor concentrations of 0.25~1.5 nM, were in the linear range of [$^{35}$S]GTP-γS binding activity. The mixtures were divided into 20 μl aliquots and further incubated with different concentrations of Ala-substituted N-Ac-ET-1(8-21) peptides or ET-1 (ranging from 10 pM to 30 μM) for 5 min at 30°C. The exchange reactions then began by adding [$^{35}$S]GTP-γS at 110 nM and incubating for 5 min at 30°C. [$^{35}$S]GTP-γS (1,250 Ci mmol$^{-1}$, PerkinElmer Life Sciences) was used after diluting with unlabeled GTP-γS to 113.6 Ci mmol$^{-1}$. The reactions were terminated by adding ice-cold stopping buffer containing 100 μM GTP in 20 mM Tris-HCl, pH 8.0, 25 mM $MgCl_2$, and 100 mM NaCl, and filtered onto cellulose-mixed ester filters in 96-well plates (multiscreen HTS HA, Merck Millipore), to isolate the G proteins from the unbound [$^{35}$S]GTP-γS. After three washes with ice-cold stopping buffer without GTP, the radioactivity of the bound [$^{35}$S]GTP-γS was measured, using a liquid scintillation counter. The assays were repeated six times. The data analyses were performed by normalizing the radioactivity counts (cpms) to values when 0 and 100% represent basal and maximal responses of ET-1(8-21), respectively. Dose-response curves were calculated by non-linear regression in GraphPad Prism 6 software. The $EC_{50}$ and $E_{max}$ values of the mutant K9A peptide in the G protein activation assay could not be determined, due to the low solubility (Table 1). Since the aforementioned G protein activation assay required at least one order of higher magnitude concentration to prepare the reaction mixtures, compared to those in the competitive ligand-binding assay. The K9A peptide solution could only be prepared at a lesser micromolar range.

For the G protein activation assay for mutant $ET_B$ receptors, GDP/[$^{35}$S]GTP-γS exchange assays were performed with membrane preparations from HEK293T cells coexpressing the wild-type or mutant $ET_B$ receptors and the rat $\alpha_{i2}$ subunit of G protein using the pcDNA3.1 vector by transfecting equal amounts of DNA[10,19]. The receptor expression levels ($B_{max}$) and $K_d$ values were determined in the saturation binding with [$^{125}$I]ET-1. The similar expressions of $\alpha_{i2}$ proteins among wild-type and mutant receptor-expressing membranes were confirmed by immunoblotting with the anti-$G_i\alpha$ 1-2 antibody (Upstate) (Figure S4). The exchange assays were carried out at 30℃ for 30 min in 100 µl of 20 mM HEPES-NaOH, at pH 7.5, and with 1 mM EDTA, 100 mM NaCl, 10 mM $MgCl_2$, 1 mM dithiothreitol, 10 µM GDP at the receptor concentration of 0.7 nM (membrane proteins 30~45 µg/ml) and eight different concentrations of ET-1 (1 pM to 1 µM). After the addition of 0.1 nM [$^{35}$S]GTP-γS (1,250 Ci/mmol, PerkinElmer Life Sciences), incubation continued for 30 min at 30℃. The reactions were stopped through the addition of ice-cold stopping buffer filtered onto glass fiber filters and measured as described above. The assays were repeated six times. The data were analyzed using GraphPad Prism 6 software as above after normalizing responses.

## RESULTS

**Alanine scan of N-acetyl [Ala$^{11,15}$]-ET-1(8-21) Peptide** To investigate the interactions responsible for the high affinity binding and receptor activation, we used the N-acetyl-[Ala$^{11,15}$]-ET-1(8-21) peptide as the wild-type and its analogs, in which the residues 8–21 were substituted by alanine individually (Table S1), instead of using mature ET-1. Owing to the two disulfide bonds between Cys$^{1}$–Cys$^{15}$ and Cys$^{3}$–Cys$^{11}$, chemical syntheses of mature ET-1 and its analogs are extremely difficult. Most of the interacting receptor residues were mapped into 8–17 helical parts to the C-terminal end 21 of ET-1 in the ET-1-bound $ET_B$ structure (Figure S1)[9]. Furthermore, the linear peptide, [Ala$^{11,15}$]-ET-1(8-21), could bind to the $ET_B$ receptor with an affinity of one order of lower magnitude, and functioned as an agonist (Figure S2, Table S2)[20,21]. We decided to select the linear peptide as the template for mature ET-1. The affinities of these peptides for $ET_B$ were examined by competitive binding for [$^{125}$I]ET-1, as shown in Table 1. The results showed that substitutions to alanine of D8, L17, D18, and I20 decreased the affinities significantly by more than two orders of magnitude, and W21 substitution caused the most severe affinity reduction of more than 1,000, suggesting the importance of D8 and the C-terminal region in the high affinity binding of ET-1 (Table 1).

In the G protein activation, D8, F14, L17, D18, and I20 substitutions revealed a highly reduced $pEC_{50}$ value, which could reflect both their binding affinities and efficacies for the $ET_B$ receptor (Table 1, Figure 1). The reduction in $pEC_{50}$ value of the F14A analog appears to depend on the reduced efficacy more than the affinity, as its reduction in affinity is relatively moderate compared to those of the D8, L17, D18, and I20 analogs. Furthermore, while V12 substitution showed a moderate but significant reduction in $pEC_{50}$ value, H16A resulted in an increase, which might be related to its binding rate to $ET_B$ because the assay was employed for only 5 min for binding, and

H16 has been suggested to maintain the appropriate structural flexibility of the C-terminal region (17-21) of ET-1[22].

**Table 1.** Competitive binding for [$^{125}$I]ET-1 and stimulation of GTPγS binding by ET-1(8-21) and analogs.

| | Competitive binding for [$^{125}$I]ET-1 | | [$^{35}$S]GTPγS binding (%) | | | |
|---|---|---|---|---|---|---|
| | $IC_{50}$ (nM) ($pIC_{50}$) | n | $EC_{50}$ (nM) | $pEC_{50}$ | $E_{max}$ | n |
| ET-1(8-21) | 6.62 ( 8.20 ± 0.09 ) | 3 | 12.3 | 7.91 ± 0.06 | 96.8 ± 2.9 | 16 |
| D8A | 520** ( 6.29 ± 0.05 ) | 4 | 1060 | 5.98 ± 0.07 **** | 87.1 ± 2.9 | 6 |
| K9A | 3.45 ( 8.47 ± 0.04 ) | 4 | N.D. | N.D. | N.D. | - |
| E10A | 51.4 ( 7.32 ± 0.08 ) | 6 | 22.6 | 7.65 ± 0.08 | 95.5 ± 3.9 | 6 |
| V12A | 18.0 ( 7.64 ± 0.07 ) | 4 | 49.3 | 7.31 ± 0.06 **** | 91.2 ± 2.4 | 6 |
| Y13A | 84.5 ( 7.07 ± 0.01 ) | 5 | 26.9 | 7.57 ± 0.10 | 72.1 ± 3.1 **** | 6 |
| F14A | 229 ( 6.65 ± 0.03 ) | 6 | 1600 | 5.80 ± 0.09 **** | 81.7 ± 4.0 * | 5 |
| H16A | 6.21 ( 8.21 ± 0.002 ) | 2 | 1.81 | 8.74 ± 0.10 **** | 96.5 ± 4.5 | 6 |
| L17A | 720*** ( 6.15 ± 0.05 ) | 3 | 494 | 6.31 ± 0.17 **** | 83.4 ± 5.8 | 5 |
| D18A | 916**** ( 6.06 ± 0.09 ) | 3 | 263 | 6.58 ± 0.09 **** | 66.5 ± 2.4 **** | 5 |
| I19A | 35.9 ( 7.45 ± 0.04 ) | 3 | 13.0 | 7.89 ± 0.12 | 100.1 ± 5.4 | 4 |
| I20A | 1690**** ( 5.79 ± 0.08 ) | 4 | 5790**** | 5.24 ± 0.09 **** | 72.7 ± 4.7 **** | 8 |
| W21A | > 10000 ( > 5.00 ) | 2 | N.D. | N.D. | N.D. | - |

Values are means ± S.E.M. (standard errors of the mean) from indicated times of independent experiments (n). Potency ($EC_{50}$ and $pEC_{50}$) and efficacy ($E_{max}$, percent of ET-1(8-21)) values were analyzed from GTPγS binding assays, as shown in Figure 1. Statistical analyses were performed by one-way analysis of variance with Dunnett's multiple comparison post hoc test. *; $p$<0.05, **; $p$<0.01, ***; $p$<0.001, ****; $p$<0.0001. n; repeated times of experiments. N.D.; not determined.

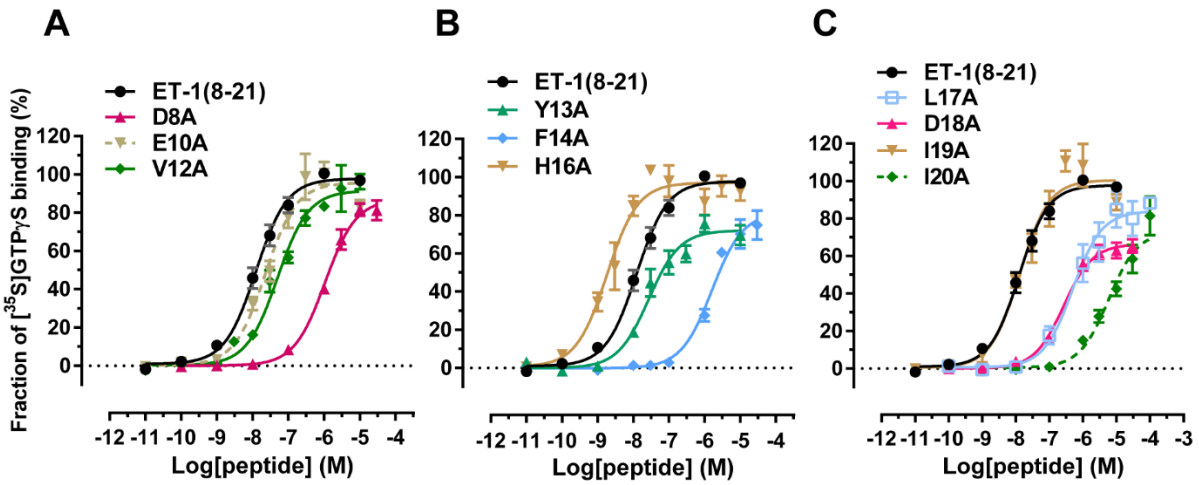

**Figure 1.** Stimulation of GTPγS binding in reconstituted HDL particles by ET-1(8-21) peptide analogs. The assays were performed with $ET_B$ in HDL at 0.7 nM, excess amounts of $\alpha_i$ and βγ subunits of G protein (Figure S3), and various concentrations of peptides, as described in experimental procedures. (A) Dose response curves by ET-1(8-21), D8A, E10A, and V12A peptide analogs are shown. (B) Dose response curves by ET-1(8-21), Y13A, F14A, and H16A. (C) Dose response curves by ET-1(8-21), L17A, D18A, I19A, and I20A. Symbols and error bars represent means and S.E.M.

In the maximal G protein activation, Y13, F14, D18, and L20 substitutions showed significantly reduced $E_{max}$ values compared to that of the wild-type ET-1(8-21), suggesting that their lack of interactions reduces the efficacies of ET-1 in G protein activation by the $ET_B$ receptor (Figure 1). Although the roles of C-terminal W21 were not explored because of its severe binding defect, the D18, I20, and W21 in the C-terminal region of ET-1 are considered to trigger structural changes via many interactions in the transmembrane binding pocket, which propagate to the cytoplasmic side of $ET_B$ in the late step of activation. On the other hand, Y13 and F14 in the helical region of ET-1 interact more with the extracellular side of the receptor (Figure 2A). Y13 interacts with $P93^{N\text{-}ter}$ and $I94^{N\text{-}ter}$ in the N-terminal tail and Y247 in the ECL2, and F14 interacts with $L361^{7.28}$, $L364^{7.31}$, and $L365^{7.32}$ at the extracellular side of TM7, both of which appear to trigger the inward movements of the N-terminal tail and TM7 required for full activation.

**G protein activation by mutant $ET_B$ receptors** To verify the contributions of Y13 and F14, the potency and efficacy of G protein activation by mutant $ET_B$ receptors were examined using mammalian cell membranes co-expressing the mutant $ET_B$ receptor and $\alpha_{i2}$ subunit of G

protein[11,19]. The mutant $ET_B$-expressing cell membranes were compared to the wild-type expressing membrane prepared in the same set of transfection. The $B_{max}$ values obtained in the saturation binding of the membranes were used as the receptor concentrations (Table 2). The expression levels of the $\alpha_{i2}$ subunit were similar to one another among the wild-type and mutants, which was confirmed by immunoblotting (Figure. S4). To verify the interaction with Y13, the G protein activation abilities of $P93A^{N\text{-}ter}$, $I94A^{N\text{-}ter}$, 93/94A, and 93/247A mutant receptors were explored (Figure 2B). All of these mutant receptors showed G protein activation reduced to 60~70% of that of the wild-type, with similar or slightly higher $pEC_{50}$ values, as the Y13A showed reduced efficacy (Figure 1). For the interaction with F14, to which $L361^{7.28}$, $L364^{7.31}$, and $L365^{7.32}$ bind, the 361/364A double mutant was examined, due to the poor expression of triple mutant, 361/364/365A. Although the defect was only moderate, it presented a lower $pEC_{50}$ value, suggesting a reduced potency (Figure 2C). Collectively, with the results of peptide analogs depicted in Figure 1, interactions between the Y13 of ET-1 and the N-terminal $P93^{N\text{-}ter}$ and $I94^{N\text{-}ter}$, and between F14 and $L361^{7.28}$/$L364^{7.31}$ are important for the formation and/or conformational equilibrium of the active state of the $ET_B$ receptor.

**Table 2.** G protein coupling of wild-type (wt) and mutant $ET_B$ receptors in HEK293T cell membranes.

| | Saturation binding | | [$^{35}$S]GTPγS binding | | |
|---|---|---|---|---|---|
| | $K_d$ (pM) | $B_{max}$ (nM) | pEC$_{50}$ | $E_{max}$ | n |
| wt | 22.8 ± 1.9 | 56.4 ± 2.0 | 9.55 ± 0.05 | 99.8 ± 2.6 | 7 |
| P93A | 26.6 ± 5.1 | 61.7 ± 5.7 | 9.88 ± 0.09 *** | 54.6 ± 2.6 *** | 6 |
| I94A | 22.6 ± 0.3 | 69.1 ± 1.8 | 9.67 ± 0.08 | 58.9 ± 2.6 *** | 6 |
| 93/94A | 30.5 ± 1.2 | 55.1 ± 2.7 | 9.86 ± 0.14 *** | 57.7 ± 4.3 *** | 6 |
| 93/247A | 26.9 ± 3.1 | 53.1 ± 0.4 | 9.58 ± 0.06 | 68.3 ± 2.4 *** | 6 |
| wt | 22.2 ± 2.0 | 85.0 ± 0.7 | 9.55 ± 0.04 | 99.8 ± 2.1 | 6 |
| 361/364A | 38.3 ± 7.6 | 97.2 ± 8.7 | 9.10 ± 0.10 *** | 91.2 ± 4.6 | 6 |

HEK293T cell membranes coexpressing ET$_B$ receptors and $\alpha_i$ protein were quantified by [$^{125}$I]ET-1 saturation binding. Values for $K_d$ and $B_{max}$ are means ± S.E.M. of two to four separate assays. Values for pEC$_{50}$ and $E_{max}$ were analyzed from GTPγS binding assays shown in Figure 2. Statistical analyses were performed by one-way analysis of variance with Dunnett's multiple comparison post hoc test. ***; $p$<0.0001. n; number of times an experiment was repeated.

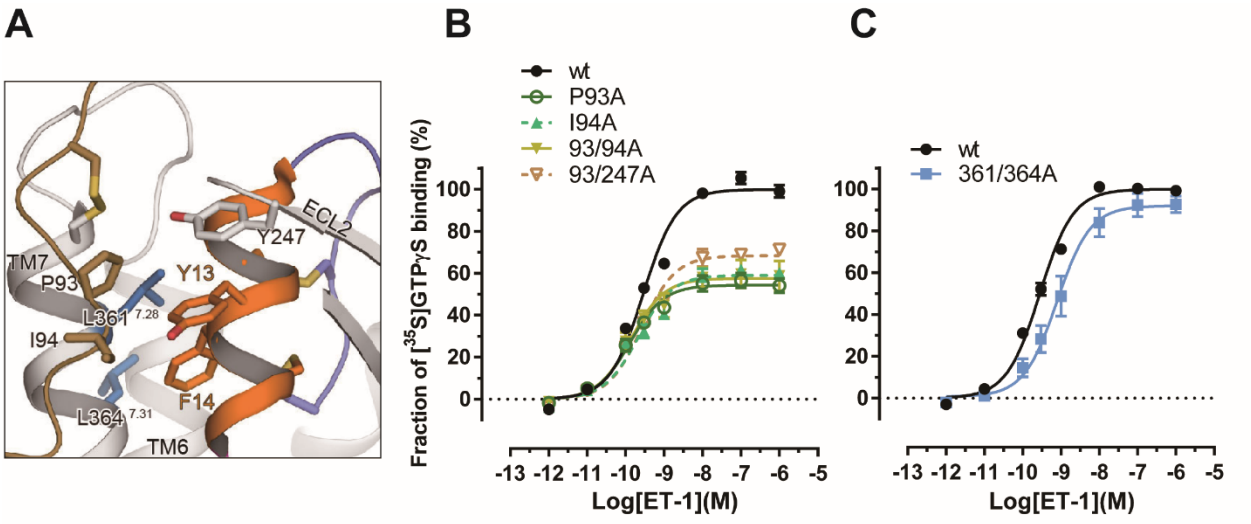


**Figure 2.** Stimulation of GTPγS binding by mutant ET$_B$ receptor in HEK293T cell membranes. G protein signaling was measured by stimulation of [$^{35}$S]GTPγS binding in HEK293T cell membranes, coexpressing ET$_B$ receptors, and $\alpha_i$ subunit of G protein. (A) The ET-1-bound ET$_B$ receptor structure around the N-terminal tail. Mutated residues in the N-terminal and TM7 are shown as green and blue sticks, respectively. The helical region of ET-1 is shown in orange. The

interacting residues are also shown as sticks. The $ET_B$ receptors with mutations in the N-terminal tail, P93A, I94A, 93/94A, and 93/247A (B), and in the extracellular side of TM7, 361/364A (C), were compared to the wild-type (wt) receptor. The receptor concentration was 0.7 nM based on the $B_{max}$ values of each membrane.

**Roles of hydrogen-bond networks in the $ET_B$ receptor** The water-mediated hydrogen bond networks are widely observed among conserved polar residues in the transmembrane domain in class A GPCRs, and their rearrangements are also observed between the inactive and active structures[4,13,14]. In addition, $Na^+$ often binds to them as a negative modulator to stabilize the inactive conformation[23]. Although $Na^+$ was not observed in the hydrogen bond network of the ligand-free and antagonist-bound $ET_B$ structures, the hydrogen bond network observed in the ET-1-bound structure is distinct from those observed in the ligand-free or antagonist-bound structures. To dissect how the observed hydrogen bonds contributed to $ET_B$ activation, we examined the well-conserved polar residues rearranged by activation; $N119^{1.50}$, $D147^{2.50}$, $S184^{3.35}$, $W336^{6.48}$, $N378^{7.45}$, and $N382^{7.49}$ (Figure 3A), using HEK293T cell membranes co-expressing mutant receptors and the $\alpha_{i2}$ subunit of G protein. The ET-1 binding affinities and concentrations of mutant receptors were confirmed by [$^{125}$I]ET-1 saturation binding (Table 3). The GDP/[$^{35}$S]GTPγS exchange assay showed that investigated mutations reduced G protein activation efficacy and, in particular, defects of $N119^{1.50}$, $D147^{2.50}$, and $N382^{7.49}$ mutations were severe (Figure 3B,C). The results suggest that the hydrogen bond network formed among these residues is important for the full activation of $ET_B$, and the direct interactions among $N119^{1.50}$, $D147^{2.50}$, and $N382^{7.49}$ are fundamental for activating G protein, contributing to the compact interactions of TM1, TM2, and TM7. The $T188A^{3.39}$ mutation could not be evaluated by the low expression of the mutant receptor.

**Table 3.** $ET_B$ receptors with polar-network mutations in HEK293T cell membranes.

| | Saturation binding | | [$^{35}$S]GTPγS binding | | |
|---|---|---|---|---|---|
| | $K_d$ (pM) | $B_{max}$ (nM) | $pEC_{50}$ | $E_{max}$ | n |
| wt | 21.2 ± 4.6 | 108 ± 0.8 | 9.60 ± 0.03 | 99.3 ± 1.7 | 7 |
| $N119A^{1.50}$ | 35.4 ± 1.1 | 41.9 ± 2.3 | 9.27 ± 0.11 | 36.0 ± 2.1 *** | 6 |
| $D147A^{2.50}$ | 31.8 ± 0.3 | 90.9 ± 7.6 | 9.22 ± 0.18 | 21.9 ± 2.0 *** | 6 |
| $W336A^{6.48}$ | 26.5 ± 3.9 | 85.0 ± 2.2 | 9.54 ± 0.07 | 69.5 ± 2.7 *** | 6 |
| $N378A^{7.45}$ | 29.0 ± 1.3 | 125 ± 6.6 | 9.65 ± 0.07 | 71.0 ± 2.8 *** | 6 |
| $N382A^{7.49}$ | 31.2 ± 2.4 | 96.3 ± 0.8 | 9.27 ± 0.09 | 43.2 ± 2.0 *** | 6 |
| wt | 22.8 ± 1.9 | 56.4 ± 2.0 | 9.67 ± 0.05 | 97.3 ± 2.5 | 7 |
| $S184A^{3.35}$ | 21.6 ± 2.7 | 50.8 ± 1.4 | 9.58 ± 0.06 | 65.2 ± 2.0 *** | 6 |
| $S379A^{7.46}$ | 25.9 ± 4.4 | 52.4 ± 1.5 | 9.42 ± 0.05 | 73.3 ± 2.2 *** | 6 |

HEK293T cell membranes coexpressing $ET_B$ receptors and $\alpha_i$ protein were quantified by [$^{125}$I]ET-1 saturation binding. Values for $K_d$ and $B_{max}$ are means ± S.E.M. of two to three separate assays. Values representing means ± S.E.M. for $pEC_{50}$ and $E_{max}$ were analyzed from GTPγS binding assays shown in Fig. 3. Statistical analyses were performed by one-way analysis of variance with Dunnett's multiple comparison post hoc test. ***; $p<0.0001$. n; number of times an experiment was repeated.

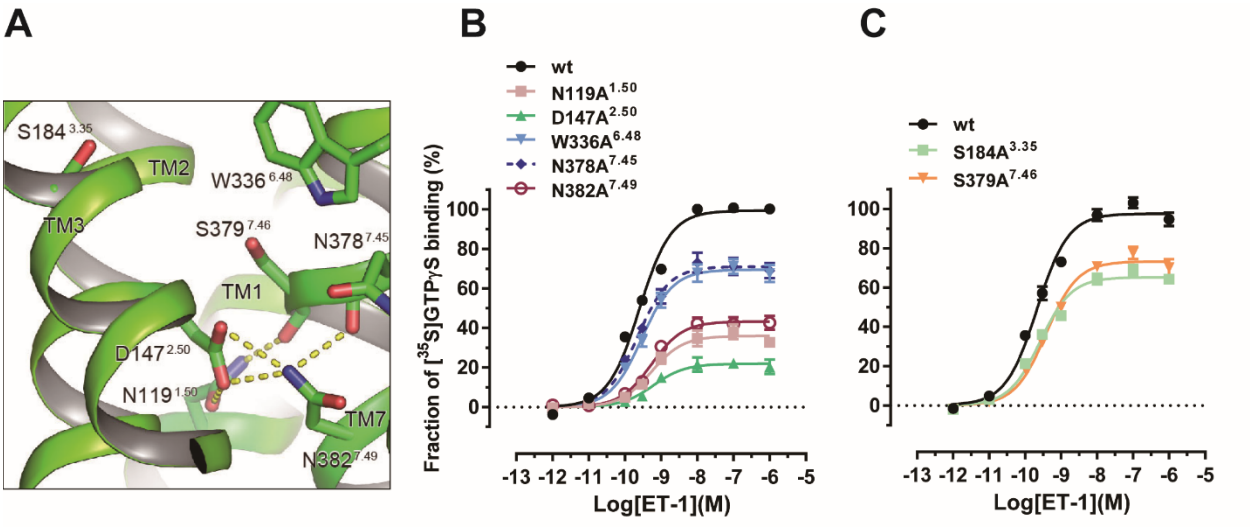


**Figure 3.** Stimulation of GTPγS binding by $ET_B$ receptors with polar-network mutations in

HEK293T cell membranes. Stimulation of [$^{35}$S]GTPγS binding in HEK293T cell membranes coexpressing $ET_B$ receptors and $\alpha_i$ subunits of G protein was measured. (A) The ET-1-bound $ET_B$ receptor structure around the polar network. All mutated residues are shown as green sticks. Hydrogen bond interactions are indicated as yellow dotted lines. The current resolution does not allow the observation of water molecules at the site. The $ET_B$ receptors with mutations of a conserved polar network[12,13], N119A$^{1.50}$, D147A$^{2.50}$, W336A$^{6.48}$, N378A$^{7.45}$, and N382A$^{7.49}$, in panel (B) and S184A$^{3.35}$ and S379A$^{7.46}$ in panel (C) were compared to the wild-type (wt) receptor. The receptor concentration employed was 0.7 nM, based on the $B_{max}$ values of each membrane.

To confirm these results, D147A$^{2.50}$, W336A$^{6.48}$, N378A$^{7.45}$, and N382A$^{7.49}$ mutant receptors were also evaluated in the *in vitro* reconstitution assay using HDL particles (Figure 4). The N119A$^{1.50}$ HDL particles could not be prepared sufficiently due to its low expression and stability during purification. The mutant receptors in the HDL particles were quantified by [$^{125}$I]ET-1 saturation binding and their G protein activation activities were measured in the presence of excess amounts of $\alpha_{i1}$ and $\beta_1\gamma_2$ subunits of G protein (Table 4). The results show reduced activities of mutant receptors, similar to those observed in the $G\alpha_i$-coexpressing membranes, with more significant defects in the N382A$^{7.49}$ and D147A$^{2.50}$ receptor HDLs, compared to the wild-type. Therefore, the hydrogen bond network formed in the transmembrane region plays an important role in the activation of $ET_B$. The HDL reconstitution assay and the assays using the $G\alpha_i$-coexpressing membranes (Figure 3) provided comparable results, although the $G\alpha_i$-coexpressing membranes have limitations in the amount of available G protein.

**Table 4.** Mutant $ET_B$ receptors in the reconstituted HDL particles.

| | Saturation binding | | [$^{35}$S]GTPγS binding | | |
|---|---|---|---|---|---|
| | $K_d$ (pM) | $B_{max}$ (nM) | $pEC_{50}$ | $E_{max}$ | n |
| wt | 27.6 ± 5.6 | 450 ± 24.1 | 9.13 ± 0.07 | 98.6 ± 3.5 | 8 |
| D147A$^{2.50}$ | 28.9 ± 5.6 | 5.4 ± 0.7 | N.A. | N.A. | 4 |
| W336A$^{6.48}$ | 24.4 ± 4.6 | 577 ± 66 | 9.20 ± 0.13 | 67.2 ± 4.1 *** | 8 |
| N378A$^{7.45}$ | 28.8 ± 5.5 | 30.4 ± 5.2 | 9.35 ± 0.11 | 77.3 ± 4.1 *** | 6 |
| N382A$^{7.49}$ | 28.3 ± 5.0 | 18.0 ± 0.2 | 9.38 ± 0.41 | 10.5 ± 1.8 *** | 7 |

Values for $K_d$ and $B_{max}$ are means ± S.E.M. of two to three separate saturation binding assays. Values and means ± S.E.M. for $pEC_{50}$ and $E_{max}$ were analyzed from GTPγS binding assays, as shown in Figure 4. Statistical analyses were performed by one-way analysis of variance with Dunnett's multiple comparison post hoc test. ***; $p<0.0001$. n; number of times an experiment was repeated. N.A., no detectable stimulation.

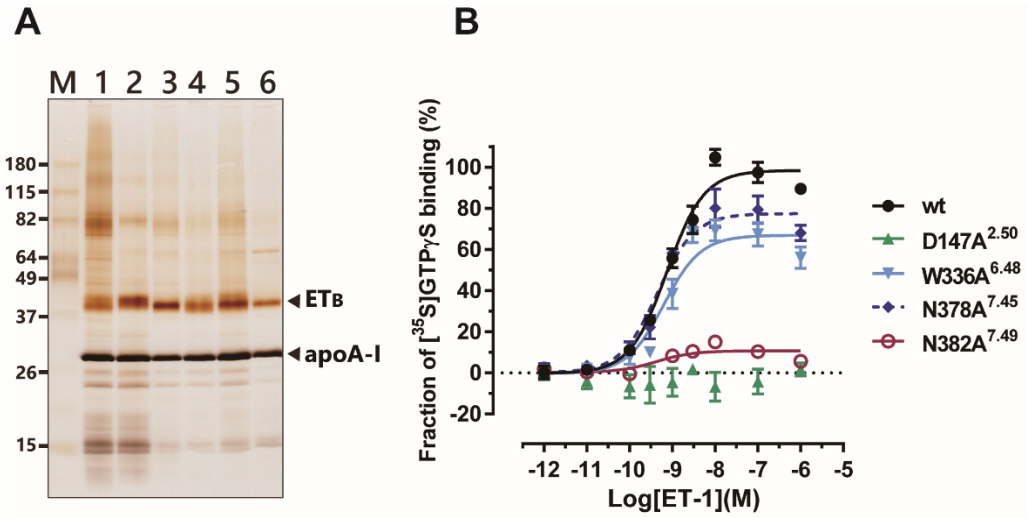


Figure 4. GTPγS binding in reconstituted HDL particles of the mutant $ET_B$ receptor. (A) Mutant $ET_B$ receptors reconstituted in HDL particles visualized by silver staining after SDS-10-20 % PAGE. Purified $ET_B$ proteins associated with the recombinant apoA-I proteins in HDLs. M, molecular markers; lane 1, N119A$^{1.50}$ (17.5%/46.2%); lane 2, D147A$^{2.50}$ (23.8%/47.7%); lane 3,

W336A$^{6.48}$ (34.2%/63.3%); lane 4, N378A$^{7.45}$ (31.5%/66.6%); lane 5, N382A$^{7.49}$ (29.4%/59.8%); lane 6, WT (21.6%/67.1%). The percentages in parentheses represent the approximate ratios of band intensities for the $ET_B$ proteins and apoA-I in total intensities in each lane, respectively, which were analyzed by CS analyzer 3.0 using the image captured by the LuminoGraph WSE-6100 equipped with the ImageSavor 6 (ATTO). (B) Stimulation of GTPγS binding in mutant HDL particles. The assays were performed with wt and mutant $ET_B$ receptors in HDLs at 0.5 nM, excess amounts of $G_i$, and various concentrations of ET-1.

## DISCUSSION

In this study, we investigate the roles of the interactions between ET-1(8-21) and $ET_B$ receptors in high affinity binding and the ability to activate G protein, based on the ET-1-bound $ET_B$ structure. The investigation of a series of alanine-substituted peptides indicated that D8, Y13, F14, L17, D18, I20, and W21 of ET-1 are important for the $ET_B$ activation, particularly D8, L17, D18, I20, and W21 for a high affinity binding, and Y13, F14, D18, and I20 for a full activation of the $ET_B$ receptor. In previous structure activity relationship studies on the *in vitro* $ET_A$ receptor binding affinity and the vena cava contractile activity, an alanine scan of ET-1 indicated that D8, Y13, F14, L17, and W21 are of major biological significance[24]. The comparison of $ET_B$ structures in the agonist-bound, ligand-free, and antagonist-bound forms allows us to examine how the interactions between ET-1 and $ET_B$ contribute to ligand binding and receptor activation. Furthermore, we studied the roles of the polar interaction network within the transmembrane domain rearranged in $ET_B$ activation, which was suggested by the structural comparison. The results indicated that the rearranged polar interactions play fundamental roles for the full activation of $ET_B$ receptor.

This study shows that interactions of Y13 and F14 are required for the full activation of $ET_B$ (Figures 1, 2), in addition to the binding of the C-terminal region to the transmembrane orthosteric site. In the ET-1 bound structure, Y13 and F14 of ET-1 interact with $ET_B$ near the extracellular side, $P93^{N\text{-term}}$ and $I94^{N\text{-term}}$, and $L361^{7.28}$, $L364^{7.31}$, and $L365^{7.32}$, respectively, resulting in the inward movement of the N-terminal tail and the extracellular side of TM7[9]. These structural changes are transmitted to the transmembrane region, in which D18, I20, and W21 in the C-terminal region of ET-1 bind to the ligand binding pocket and change helical interactions of $ET_B$ further. In particular, the D18 side chain interacts with $R343^{6.55}$ and $D368^{7.35}$, leading to the formation of an electrostatic interaction network that includes the C-terminal carboxylate, $K182^{3.33}$, and $K273^{5.38}$, which results in the inward shift of TM6 and TM7, and tight packing of the helical core of TM3, 5, 6, and 7[9] (Figure S5). Similarly, the side chain of I20 interacts with $I157^{2.60}$ and $P178^{3.29}$, and its backbone amide and carbonyl form hydrogen bonds with $N158^{2.61}$ and $Q181^{3.32}$, respectively, contributing to the inward shift of TM2 and tight association of TM2 with TM3. In addition, the side chain of W21 interacts directly with $K182^{3.33}$ and $W336^{6.48}$ in the CWxP motif, which is considered a signal transmission switch in class A GPCR. Therefore, the interactions of D18, I20, and W21 contribute to changed helical interactions of TM2, 3, 5, 6, and 7 of $ET_B$ in receptor activation. The interactions of ET-1(18-21) with the transmembrane ligand binding pocket of $ET_B$ appear to correspond to the orthosteric binding of small endogenous agonists, such as adrenalin or adenosine[25,26]. Nonetheless, these are not sufficient, and the additional interactions by Y13 and F14 of ET-1 near the extracellular side play auxiliary roles for the full activation of $ET_B$.

The reduced efficacy patterns of Y13A/ $P93A^{N\text{-ter}}$ and $I94A^{N\text{-ter}}$ correspond to the “affinity-dominant” and those of F14A/$L361A^{7.28}$/$L364A^{7.31}$ resembled the “efficacy-dominant” partial

agonist-type[27]. While both interactions may affect the conformational equilibrium of $ET_B$, their detailed functions in $ET_B$ activation do not appear to be the same. $P93^{N\text{-}ter}$ and $I94^{N\text{-}ter}$ were originally located at the extracellular end of TM1(93-127) in the ligand-free and antagonist-bound structures (Figure S1B) [9,10]. Upon ET-1 binding, the α-helical structure of this region (93-97) of TM1 collapses and $P93^{N\text{-}ter}$ and $I94^{N\text{-}ter}$ move inward, while the new end of TM1, $E98^{1.29}$, moves outward by approximately 4.4 Å to accommodate the inward movement of TM2[9]. P93 not only interacts with Y13, but also may facilitate the helical collapse of TM1 to increase the flexibility of the N-terminal tail. In the ET-3-bound $ET_B$ structure, the side chain of $P93^{N\text{-}ter}$ does not appear to directly interact with Y13[28], suggesting its structural role. F14 interacts with $L361^{7.28}$, $L364^{7.31}$, and $L365^{7.32}$ at the extracellular side of TM7. Because all interactions with F14 could not be excluded by the receptor mutations due to the low expression level of the triple mutant receptor, the extent of the defects in the $pEC_{50}$ value of L361/364A in the G protein activation assay is moderate (Figure 2). However, the reduced potencies ($pEC_{50}$) of both the L361/364A mutant receptor and F14A peptide analog suggest that the inward movement of the extracellular side of TM7 is essential for a full activation of the receptor. In addition, the movements of the N-terminal tail and TM7 were further stabilized by a disulfide bond between $C90^{N\text{-}term}$ and $C358^{7.25}$ and, thus, propagated to the transmembrane helical region in an early step of receptor activation.

Upon ET-1 binding, the inward movements of the N-terminal tail, TM2, TM6, and TM7, of $ET_B$ lead to the rearranging of the network of polar interactions among the transmembrane helices, including water molecules. These polar networks are formed among conserved polar residues and the backbone, observed in a number of GPCR crystal structures[13,14]. In $ET_B$, the lack of hydrogen bonds by mutations of the residues, $S184^{3.35}$, $W336^{6.48}$, $N378^{7.45}$, and $S379^{7.46}$ resulted in reduced efficacy (Figures 3, 4), suggesting that the full activation of $ET_B$ requires coordinated

rearrangements of the polar network upon agonist binding. These findings correspond with the structure of IRL1620, a partial agonist-bound $ET_B$, in which rearrangement of the polar interaction network is partly incomplete and water-mediated interactions between $D147^{2.50}$ and $W336^{6.48}$ are preserved[28]. Furthermore, the residues $N119^{1.50}$, $D147^{2.50}$, and $N382^{7.49}$ form direct hydrogen bonds with one another via the inward shift of the cytoplasmic side of TM7 and play central roles in G protein activation (Figures 3, 4). The replacement of $D^{2.50}$ has also been shown to lose signaling activity in $ET_B$ and other class A GPCRs[29-31]. These results suggest that the inward shift of the cytoplasmic side of TM7 is an important driving force for receptor activation, featured as the outward movement of the cytoplasmic side of TM6[4].

The coordinated movements between the N-terminal tail and the extracellular side of TM7 might be a common part of the early activation process in class A GPCRs for mid-sized endogenous agonists. In the angiotensin II type 1 and type 2 receptors ($AT_1R$ and $AT_2R$), partial agonist [$Sar^1$,$Ile^8$]AngII-bound structures showed that the N-terminus of [$Sar^1$,$Ile^8$]AngII was close to the N-terminal tail of the receptor, and the second arginine interacted with the extracellular side of TM7[6,7]. In the neurotensin receptor, the modified peptide agonist $NTS_{8-13}$ (RRPYIL) also interacted with the N-terminal tail and the extracellular side of the TM7 in the complex structures[8,32]. The N-terminal tail of the apelin receptor interacts with the 17 amino acid residue-long modified peptide agonist closely[33]. The viral chemokine receptor, US28, interacts with the chemokine CX3CL1 more extensively, using the exterior N-terminal tail and extracellular domain (site 1) and the transmembrane binding pockets (site2), consistent with a two-site model[34,35]. In contrast, the modified peptide agonist, DAMGO (H-Tyr-D-Ala-Gly-N(Me)Phe-Gly-OH), does not interact with the N-terminal tail or the extracellular side of TM7 of the μ-opioid receptor in the active conformation[5]. While ligand size influences the activation mechanism, interactions near the

extracellular side by relatively large agonists could provide efficacious activation modes, which could be developed as an allosteric site in drug design in addition to the transmembrane orthosteric interactions.

Class B GPCRs also bind to the peptide hormones that comprise around 27–45 amino acid residues and are essential for physiological processes. They contain a characteristic large extracellular N-terminal domain (NTD) and a transmembrane helical domain, both of which are involved in ligand-binding, as reported by extensive biological and structural studies (36-41). In contrast to $ET_B$, the NTD interacts with the C-terminus of the peptide ligand for initiating peptide recognition, and the transmembrane helical domain forms the N-terminus of the peptide-binding pocket to activate the receptor. Furthermore, the interactions of the stalk region between the NTD and TM1, ECL1, and ECL2 with a peptide agonist are implicated in a full activation of the receptor by studying the partial agonists of the glucagon-like peptide-1 (GLP-1) and comparing the inactive and active structures of the calcitonin receptor, glucagon receptor, and GLP-1 receptor (GLP-1R) (37-40). The structural comparison in class B GPCRs suggested that agonist binding induced the outward shifts of TM6 and TM7 and an inward shift of TM1 on the extracellular sides of GLP-1R and calcitonin receptor, which are different from those observed in the $ET_B$ receptor and other class A GPCRs with a tendency to narrow the ligand-binding pocket (9, 39-42). Therefore, the extracellular sides of the class B GPCRs receptor also play crucial roles in interaction with the peptide ligand and the full activation of the receptor, and their signal propagation mechanisms within the transmembrane helical bundle diverge from the class A GPCRs, although the final outward movements of TM6 in the cytoplasmic side with the active conformation interacting with a G protein have been also observed in the class B GPCRs (39-41) .

In conclusion, we found that the endogenous peptide agonist ET-1 shifts the conformational equilibrium of the $ET_B$ receptor towards the active state efficiently via both interactions with the N-terminal tail and extracellular side of TM7, and within the transmembrane binding pocket accompanied by precise rearrangements of the polar interaction network. The results provide an activation mechanism of $ET_B$ by mid-size peptide agonist ET-1 and a clue for optimization of $ET_B$ receptor agonists.

ASSOCIATED CONTENT

**Supporting Information**

Supplemental figures and tables (PDF)

**Accession Codes**

UniProt ID, human endothelin receptor type B, P24530.

AUTHOR INFORMATION

Corresponding Author

*Department of Biophysics, Graduate School of Science, Kyoto University, Kitashirakawa, Oiwake, Sakyo, Kyoto 606-8502, Japan

Phone: +81-75-753-4216, Fax: +81-75-753-4218; E-mail: doi@mb.biophys.kyoto-u.ac.jp

Present Address

†Department of Physiology, Graduate School of Medicine, The University of Tokyo, Bunkyo, Tokyo 113-0033, Japan

ORCID

Tomoko Doi: 0000-0002-6568-4576

Kazutoshi Tani: 0000-0003-4835-154X

Author Contributions

K.T. and T.D. participated in the study design. K.K. and T.D. performed the experiments. All authors analyzed the data and contributed to the writing of the manuscript.

Funding

This work was supported by JSPS KAKENHI Grant number 16K07172 and 20H03210, and ISHIZUE 2019 of Kyoto University Research Development Program.

Notes

The authors declare no competing financial interest.

ACKNOWLEDGMENT

The authors thank Dr. Yoshinori Fujiyoshi for critical reading of the manuscript and his encouragement during the project.

ABBREVIATIONS

ET, endothelin; $ET_A$, endothelin type-A receptor; $ET_B$, endothelin type-B receptor; ECL, extracellular loop; GPCRs, G protein-coupled receptors; NTD, N-terminal domain; rHDLs, reconstituted high-density lipoprotein particles; apoA-I, apolipoprotein A-I; S.E.M., standard errors of the mean

REFERENCES

(1) Kedzierski, R. M. and Yanagisawa, M. (2001) Endothelin system: The double-edged swords in health and disease. *Annu. Rev. Pharmacol. Toxicol. 41*, 851-876.

(2) Davenport, A. P., Hyndman, K. A., Dhaun, N., Southan, C., Kohan, D. E., Pollock,

J. S., Pollock, D. M., Webb, D. J., and Maguire, J. J. (2016) Endothelin. *Phamacol. Rev. 68*, 357-418.

(3) Wu, F., Song, G., de Graaf, C., and Stevens, R.C. (2017) Structure and Function of Peptide-Binding G Protein-Coupled Receptors. *J. Mol. Biol. 429*, 2726-2745.

(4) Weis, W. I. and Kobilka, B. K. (2018) The molecular basis of G protein-coupled receptor activation. *Annu. Rev. Biochem. 87*, 897-919.

(5) Koehl, A., Hu, H., Maeda, S., Zhang, Y., Qu, Q., Paggi, J. M., Latorraca, N. R., Hilger, D., Dawson, R., Matile, H., Schertler, G. F. X., Granier, S., Weis, W. I., Dror, R. O., Manglik, A., Skiniotis, G., and Kobilka, B. K. (2018) Structure of the μ-opioid receptor-$G_i$ protein complex. *Nature 558*, 547-552.

(6) Asada, H., Horita, S., Hirata, K., Shiroishi, M., Shiimura, Y., Iwanari, H., Hamakubo, T., Shimamura, T., Nomura, N., Kusano-Arai, O., Uemura, T., Suno, C., Kobayashi, T., and Iwata, S. (2018) Crystal structure of the human angiotensin II type 2 receptor bound to an angiotensin II analog. *Nat. Struct. Mol. Biol. 25*, 570-576.

(7) Wingler, L. M., McMahon, C., Staus, D. P., Lefkowitz, R. J., Kruse, A. C. (2019) Distinctive activation mechanism for angiotensin receptor revealed by a synthetic nanobody. *Cell 176*, 479-490.

(8) Kato, H. E., Zhang, Y., Hu, H., Suomivuori, C.-M., Kadji, F. M. N., Aoki, J., Kumar, K., Fonseca, R., Hilger, D., Huang, W., Latorraca, N. R., Inoue, A., Dror, R. O., Kobilka, B. K., and

Skiniotis, G. (2019) Conformational transitions of a neurotensin receptor 1-$G_{i1}$ complex. *Nature 572*, 80-85.

(9) Shihoya, W., Nishizawa, T., Okuta, A., Tani, K., Dohmae, N., Fujiyoshi, Y., Nureki, O., and Doi, T. (2016) Activation mechanism of endothelin $ET_B$ receptor by endothelin-1. *Nature 537*, 363-368.

(10) Shihoya, W., Nishizawa, T., Yamashita, K., Inoue, A., Hirata, K., Kadji, F. M. N., Okuta, A., Tani, K., Aoki, J., Fujiyoshi, Y., Doi, T., and Nureki, O. (2017) X-ray structures of endothelin $ET_B$ receptor bound to clinical antagonist bosentan and its analog. *Nat. Struct. Mol. Boil. 24*, 758-764.

(11) Lane, J. R., Powney, B., Wise, A., Rees, S., and Milligan, G. (2008) G protein coupling and ligand selectivity of the D2L and D3 dopamine receptors. *J. Pharmacol. Exp. Ther. 325*, 319–330.

(12) Ballesteros, J. and Weinstein, H. (1995) Integrated methods for the construction of three dimensional models and computational probing of structure-function relations in G protein-coupled receptors. *Methods Neurosci. 25*, 366-428.

(13) Huang, W., Maglik, A., Venkatakrishnan, A. J., Laeremans, T., Feinberg, E. N., Sanborn, A. L., Kato, H. E., Livingston, K. E., Thorsen, T. S., Kling, R. C., Granier, S., Gmeiner, P., Husbands, S. M., Traynor, J. R., Weis, W. I., Steyaert, J., Dror, R. O., and Kobilka, B. K. (2015) Structural insights into μ-opioid receptor activation. *Nature 524*, 315-321.

(14) Venkatakrishnan, A. J., Ma, A. K., Fonseca, R., Latorraca, N. R., Kelly, B., Betz, R. M., Asawa, C., Kobilk, B. K., and Dror, R. O. (2019) Diverse GPCRs exhibit conserved water networks for stabilization and activation. *Proc. Natl. Acad, Sci. U. S. A. 116,* 3288-3293.

(15) Pace, C. N., Vajdos, F., Fee, L., Grimsley, G., and Gray, T. (1995) How to measure and predict the molar absorption coefficient of a protein. *Protein Sci. 4,* 2411-2423.

(16) Ritchie, T. K., Grinkova, Y. V., Bayburt, T. H., Denisov, I. G., Zolnerciks, J. K., Atkins, W. M., and Sligar, S. G. (2009) Reconstitution of membrane proteins in phospholipid bilayer nanodiscs. *Methods Enzymol. 464*, 211-231.

(17) Whorton, M. W., Bokoch, M. P., Rasmussen, S. G. F., Huang, B., Zare, R. N., Kobilka, B. K., Sunahara, R. K. (2007) A monomeric G protein-coupled receptor isolated in a high-density lipoprotein particle efficiently activates its G protein. *Proc. Natl. Acad. Sci. U. S. A. 104*, 7682-7687.

(18) Vélez-Ruiz, G. A. and Sunahara, R. K. (2011) Reconstitution of G protein-coupled receptors into a model bilayer system: reconstituted high-density lipoprotein particles, *Methods Mol. Biol. 756*, 167-182.

(19) Manglik, A., Lin, H., Aryal, D. K., McCorvy, J. D., Dengler, D., Corder, G., Levit, A., Kling, R. C., Bernat, V., Hübner, H., Huang, X.-P., Sassano, M. F., Giguère, P. M., Löber, S., Duan, D., Scherrer, G., Kobilka, B. K., Gmeiner, P., Roth, B. L., and Shoichet, B. K. (2016) Structure-based discovery of opioid analgesics with reduced side effects. *Nature 537,* 185-190.

(20) Takai, M., Umemura, I., Yamasaki, K., Watakabe, T. , Fujitani, Y., Oda, K., Urade, Y., lnui, T., Yamamura, T., and Okada T. (1992) A potent and specific agonist, Suc-[Glu$^{9}$, Ala$^{11,15}$]-

endothelin-1(8-21), IRL1620, for the $ET_B$ receptor. *Biochem. Biophys. Res. Commun. 184*, 953-959.

(21) Saeki, T., Ihara, M., Fukuroda, T., Yamagiwa, M., and Yano, M. (1991) [$Ala^{1,3,11,15}$]endothelin-1 analogs with $ET_B$ agonistic activity. *Biochem. Biophys. Res. Commun. 179*, 286-292.

(22) Hiramatsu, H., Aduma, H., Tanaka, Y., Miura, T., and Takeuchi, H. (2010) Role of His16 in the structural flexibility of the C-terminal region of human endothelin-1. *J. Mol. Struc. 976*, 328-332.

(23) Zarzycka, B., Zaidi, S. A., Roth, B. L., and Katritch, V. (2019) Harnessing ion-binding sites for GPCR pharmacology. *Pharmacol. Rev. 71*, 571-595.

(24) Tam, J. P., Liu, W., Zhang, J.-W., Galantino, M., Bertolero, F., Cristiani, C., Vaghi, F., and DE Castiglione, R. (1994) Alanine scan of endothelin: importance of aromatic residues. *Peptides 15*, 703-708.

(25) Ring, A. M., Manglik, A., Kruse, A. C., Enos, M. D., Weis, W. I., Garcia, K. C., and Kobilka, B. K. (2013) Adrenaline-activated structure of $\beta_2$-adrenoceptor stabilized by an engineered nanobody. *Nature 502*, 575-579.

(26) Lebon, G., Warne, T., Edwards, P. C., Bennett, K., Langmead, C. J., Leslie, A. G. W., and Tate, C. G. (2011) Agonist-bound adenosine $A_{2A}$ receptor structures reveal common features of GPCR activation. *Nature 474*, 521-525.

(27) Kenakin, T. P. (2018) A pharmacology primer. *Acad. Press.*

(28) Shihoya, W., Izume, T., Inoue, A., Yamashita, K., Kadji, F. M. N., Hirata, K., Aoki, J., Nishizawa, T., and Nureki, O. (2018) Crystal structures of human $ET_B$ receptor provide mechanistic insight into receptor activation and partial activation. *Nat. Commun. 9*, 4711-4721.

(29) Rose, P. M., Krystek Jr., S. R., Patel, P. S., Liu, E. C. K., Lynch, J. S., Lach, D. A., Fisher, S. M., and Webb, M. L. (1995) Aspartate mutation distinguishes $ET_A$ but not $ET_B$ receptor subtype-selective ligand binding while abolishing phospholipase C activation in both receptors. *FEBS Lett. 361*, 243-249.

(30) Massink, A., Gutiérrez-de-Terán, H., Lenselink, E. B., Zacarías, N. V. O., Xia, L., Heitman, L. H., Katritch, V., Stevens, R. C., and IJzerman, A. P. (2015) Sodium ion binding pocket mutations and adenosine $A_{2A}$ Receptor Function. *Mol. Pharmacol 87*, 305-313.

(31) White, K. L., Eddy, M. T., Gao, Z.-G., Han, G. W., Lian, T., Deary, A., Patel, N., Jacobson, K. A., Katritch, V., and Stevens, R. C. (2018) Structural connection between activation microswitch and allosteric sodium site in GPCR signaling. *Structure 26*, 259-269.

(32) Krumm, B. E., White, J. F., Shah, P., and Grisshammer, R. (2015) Structural prerequisites for G-protein activation by the neurotensin receptor. *Nat. Commun. 6*, 7895-7904.

(33) Ma, Y., Yue, Y., Ma, Y., Zhang, Q., Zhou, Q., Song, Y., Shen, Y., Li, X., Ma, X., Li, C., Hanson, M. A., Han, G. W., Sickmier, E. A., Swaminath, G., Zhao, S., Stevens, R. C., Hu, L. A., Zhong, W., Zhang, M., and Xu, F. (2017) Structural Basis for Apelin Control of the Human Apelin Receptor. *Structure 25*, 858-866.

(34) Burg, J. S., Ingram, J. R., Venkatakrishnan, A. J., Jude, K. M., Dukkipati, A., Feinberg, E. N., Angelini, A., Waghray, D., Dror, R. O., Ploegh, H. L., and Garcia, K. C. (2015) Structural

basis for chemokine recognition and activation of a viral G protein-coupled receptor. *Science 347*, 1113-1117.

(35) Thiele, S. and Rosenkilde, M. M. (2014) Interaction of Chemokines with their Receptors - From Initial Chemokine Binding to Receptor Activating Steps. *Curr. Med. Chem. 21*, 3594-3614.

(36) Culhane, K. J., Liu, Y., Cai, Y., and Yan, E.C. (2015) Transmembrane signal transduction by peptide hormones via family B G protein-coupled receptors. *Front. Pharmacol. 6*, 264.

(37) Can Cao, C., Zhang, H., Yang, Z., and Wu, B. (2018) Peptide recognition, signaling and modulation of class B G protein-coupled receptors. *Curr. Opin. Struct. Biol. 51*, 53–60.

(38) Zhang, H., Qiao, A., Yang, D., Yang, L., Dai, A., de Graaf, C., Reedtz- Runge, S., Dharmarajan, V., Han, G. W., Grant, T. D., Sierra, R. G., Weierstall, U., Nelson, G., Liu, W., Wu, Y., Ma, L., Cai, X., Lin, G., Wu, X., Geng, Z., Dong, Y., Song, G., Griffin, P. R., Lau, J., Cherezov, V., Yang, H., Hanson, M. A., Stevens, R. C., Zhao, Q., Jiang, H., Ming-Wei Wang, M.-W., and Wu, B. (2017) Structure of the full-length glucagon class B G-protein-coupled receptor. *Nature 546*, 259-264.

(39) Zhang, Y., Sun, B., Feng, D., Hu, H., Chu, M., Qu, Q., Tarrasch, J. T., Li, S., Kobilka, T. S., Kobilka, B. K., and Skiniotis, G. (2017) Cryo-EM structure of the activated GLP-1 receptor in complex with a G protein. *Nature 546*, 248-253.

(40) Jazayeri, A., Rappas, M., Brown, A. J. H., Kean, J., Errey, J. C., Robertson, N. J., Fiez-Vandal, C., Andrews, S. P., Congreve, M., Bortolato, A., Mason, J. S., Baig, A. H., Teobald, I., Doré, A. S., Weir, M., Cooke, R. M., and Marshall, F. M. (2017) Crystal structure of the GLP-1 receptor

bound to a peptide agonist. *Nature 546*, 254-258.

(41) Liang, Y. L., Khoshouei, M., Radjainia, M., Zhang, Y., Glukhova, A., Tarrasch, J., Thal, D. M., Furness, S. G. B., Christopoulos, G., Coudrat, T., Danev, R., Baumeister, W., Miller, L. J., Christopoulos, A., Kobilka, B. K., Wootten, D., Skiniotis, G., and Sexton, P. M. (2017) Phase-plate cryo-EM structure of a class B GPCR-G-protein complex. *Nature 546*, 118-123.

(42) Dalton, J. A., Lans, I., and Giraldo, J. (2015) Quantifying conformational changes in GPCRs: glimpse of a common functional mechanism. *BMC Bioinformatics 16*, 124.

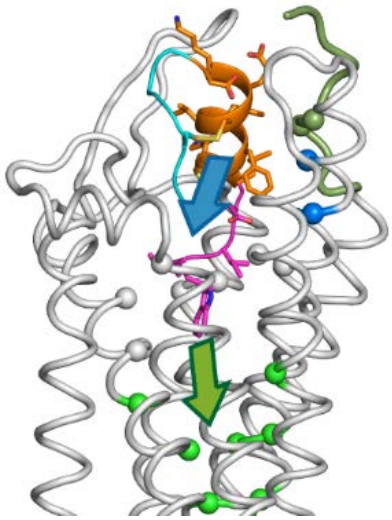

For Table of Contents Only

Supplemental Data

# Characterization of Critical Residues in the Extracellular and Transmembrane Domains of the Endothelin Type-B Receptor for Propagation of the Endothelin-1 Signal

Tomoko Doi,[1*] Kohei Kikuta,[1] and Kazutoshi Tani[2]

[1]Department of Biophysics, Graduate School of Science, Kyoto University, Kyoto 606-8502, Japan
[2]Graduate School of Medicine, Mie University, 2-174 Edobashi, Tsu, Mie 514-8507, Japan

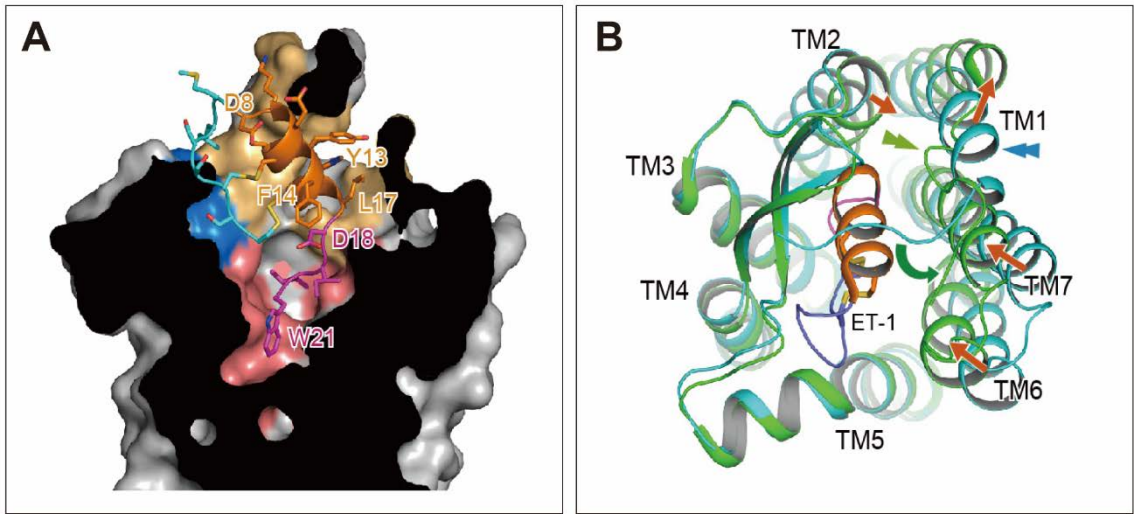


Figure S1. The ET-1-$ET_B$ receptor interactions and structural comparison of the $ET_B$ receptors. (A) Cutaway surface representation of the $ET_B$ receptor in a complex with ET-1. Residues of the ET-1 are represented as cyan- (N-terminal region; 1-7), orange- (Helical region; 8-17), and magenta-colored sticks (C-terminal region; 18-21). The receptor residues that interact with the N-terminal, helical, and C-terminal regions of ET-1 are colored in marine, light orange, and salmon, respectively. (B) Extracellular views of the ET-1-bound (green) and ligand-free (cyan) $ET_B$ receptor. Red and green arrows indicate the ET-1-induced movements of the TM helices and the N-terminal part, respectively. Double arrow heads indicate that ET-1 induced the secondary conformational change in the N-terminal of the receptor.

Table S1. Amino acid sequence of ET-1 and peptide analogues

| ET-1 | 1 5 10 15 20<br>CSCSSLMDKECVYFCHLDIIW |
|---|---|
| **ET-1(8-21)** | **N-Ac-DKEAVYFAHLDIIW** |
| **D8A** | N-Ac-**A**KEAVYFAHLDIIW |
| **K9A** | N-Ac-D**A**EAVYFAHLDIIW |
| **E10A** | N-Ac-DK**A**AVYFAHLDIIW |
| **V12A** | N-Ac-DKEA**A**YFAHLDIIW |
| **Y13A** | N-Ac-DKEAV**A**FAHLDIIW |
| **F14A** | N-Ac-DKEAVY**A**AHLDIIW |
| **H16A** | N-Ac-DKEAVYFA**A**LDIIW |
| **L17A** | N-Ac-DKEAVYFAH**A**DIIW |
| **D18A** | N-Ac-DKEAVYFAHL**A**IIW |
| **I19A** | N-Ac-DKEAVYFAHLD**A**IW |
| **I20A** | N-Ac-DKEAVYFAHLDI**A**W |
| **W21A** | N-Ac-DKEAVYFAHLDII**A** |

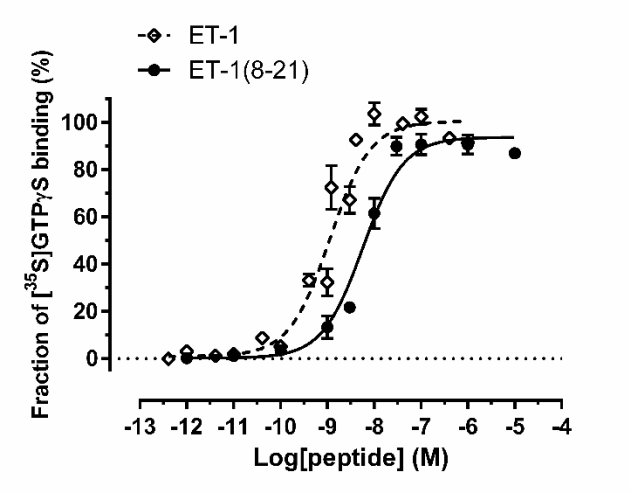


Figure S2. Stimulation of GTP-γS binding in reconstituted HDL particles by ET-1 and ET-1(8–21)

The assays were performed with $ET_B$ in 0.7 nM HDL and excess amounts of $\alpha_i$ and βγ subunits of G protein (Figure S3), as described in the experimental procedures. The analyzed values for $EC_{50}$ and $E_{max}$ are summarized in Table S2.

Table S2. Binding affinity and stimulation of GTP-γS binding by ET-1 and ET(8-21)

| | Competitive binding for [$^{125}$I]ET-1 | | $^{35}$S]GTPγS binding (%) | | | |
|---|---|---|---|---|---|---|
| | $IC_{50}$ (nM) ($pIC_{50}$) | n | $EC_{50}$ (nM) | $pEC_{50}$ | $E_{max}$ | n |
| ET-1 | 0.30 ( 9.53 ± 0.04 ) | 3 | 1.1 | 8.95 ± 0.07 | 99.7 ± 3.7 | 6 |
| ET(8-21) | 6.62 ( 8.20 ± 0.09 ) | 3 | 5.7 | 8.24 ± 0.08 | 93.6 ± 3.5 | 4 |

The experiments were performed as described in the experimental procedures, Table 1 and Figure S2.

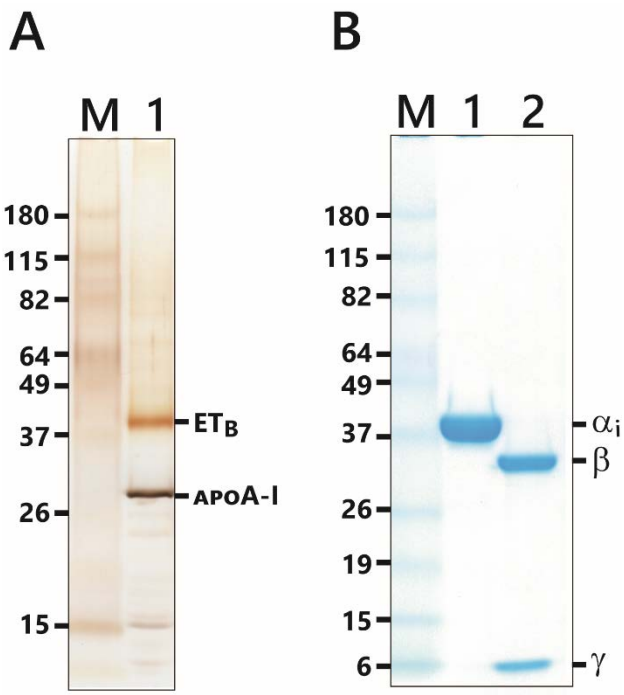


Figure S3. Reconstituted wild-type $ET_B$ receptors in HDL particles (A) and purified $G_i$ proteins (B). (A) The HDL particles containing wild-type $ET_B$ (lane 1) were visualized by silver staining after 10-20% SDS-PAGE. (B) Purified $\alpha_i$ subunit (lane 1) and $\beta\gamma$ subunits (lane 2) were visualized by C.B.B. staining.

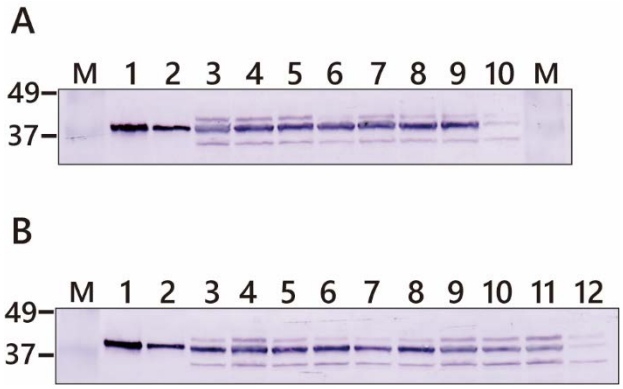


Figure S4. G protein $\alpha_{i2}$ subunit proteins co-expressed with $ET_B$ receptors in HEK293T cell membranes analyzed by immunoblotting. Each $\alpha_{i2}$ protein in the wild-type or mutant receptor-expressing membranes were at a similar level to one another. (A) The cell membranes assayed in Figure 2, containing wild-type or mutant $ET_B$ receptors at 0.6 pmol based on their $B_{max}$ (25~40 μg proteins per lane), were analyzed in the same order as specified in Table 2. Lane 1, purified $\alpha_{i1}$ subunit ~80 ng; lane 2, purified $\alpha_{i1}$ subunit ~40 ng; lane 3, wild-type $ET_B$; lane 4, P93A; lane 5, I94A; lane 6, 93/94A; lane 7, 93/247A; lane 8, wild-type $ET_B$; lane 9, 361/364A; lane 10, untransfected cell membranes containing 25 μg protein. (B) The cell membranes assayed in Figure 3 containing wild-type or mutant $ET_B$ receptors in the same amounts as in A were analyzed in the same order as specified in Table 3. Lane 1, purified $\alpha_{i1}$ subunit ~80 ng; lane 2, purified $\alpha_{i1}$ subunit ~40 ng; lane 3, wild-type $ET_B$; lane 4, N119A; lane 5, D147A; lane 6, W336A; lane 7, N378A; lane 8, N382A; lane 9, wild-type $ET_B$; lane 10, S184A; lane 11, S379A; lane 12, untransfected cell membranes containing 25 μg protein.

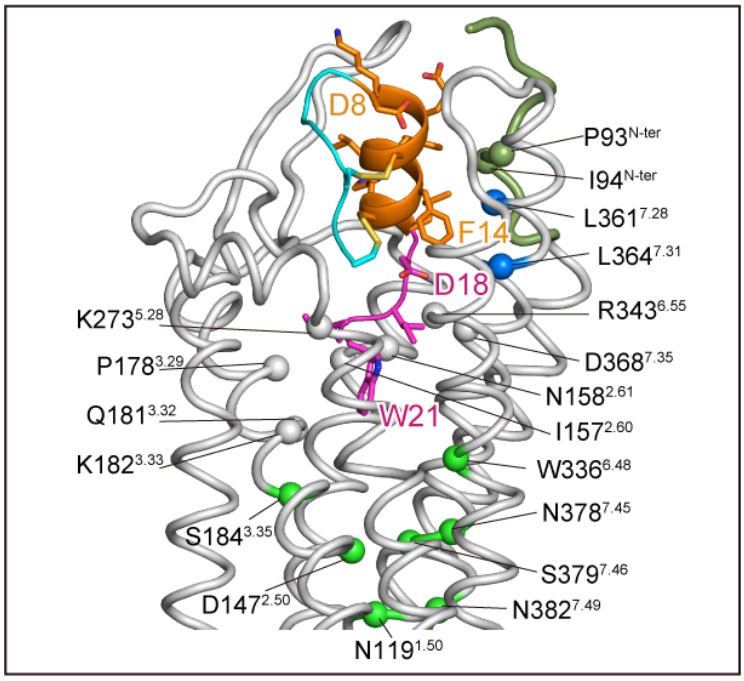


Figure S5. The ET-1 bound $ET_B$ receptor structure with critical residues for interactions. Color codes of the ET-1 are the same as in Figure S1A. Color codes of the receptor residues are the same as in Figures 2A and 3A. Gray spheres of the $ET_B$ receptor represent the residues interacting with the C-terminal region of ET-1.